J Nanostruct 16(4): 4890-4900, Autumn 2026

RESEARCH PAPER

Synthesis and Structural Characterization of a Zeolite-Incorporated Carboxymethyl Cellulose Hydrogel for Safranin O Adsorption: Equilibrium, Kinetics, Thermodynamics and Reusability

Walaa Mohammed Najem

Faculty of Pharmacy, Jabir Ibn Hayyan University for Medical and Pharmaceutical Sciences, Najaf Ashraf, Iraq

ARTICLE INFO

Article History:
Received 17 May 2026
Accepted 25 July 2026
Published 01 October 2026

Keywords:
Adsorption
Carboxymethyl cellulose
Hydrogel composite
Wastewater treatment
Zeolite, Safranin O

ABSTRACT

Study reports the synthesis and detailed nano-scale characterization of a new biopolymer composite, (CMC-AAC-co-HEAM)-g-zeolite, prepared by free-radical graft polymerization and tested as an adsorbent for safranin O (Saf) in water. Carboxymethyl cellulose (CMC) was used as the backbone; acrylic acid (AAc) and hydroxyethyl acrylamide (HEAM) were grafted onto it with potassium persulfate (KPS) as initiator and N, N′-methylenebisacrylamide (MBA) as crosslinker, and natural zeolite was added to raise porosity and the density of active sites. Characterization relied on FTIR, XRD, FESEM, TEM, BET, TGA, and zeta potential measurements. The batch experiments looked at how contact time, adsorbent dose, pH, temperature, and ionic strength influenced Saf uptake. Of the isotherms tested, the Freundlich model described the equilibrium data best (R^2 = 0.987), which points to a heterogeneous, multilayer process, whereas the kinetics followed a pseudo-second-order rate law (R^2 ≈ 1.000). The Langmuir equation gave a maximum capacity of 271.19 mg g^{-1}. Thermodynamic analysis showed the uptake to be exothermic ($\Delta H < 0$) and spontaneous ($\Delta G < 0$). After four adsorption-desorption cycles, the composite still removed about 87% of the dye. Overall, these results suggest the zeolite-grafted hydrogel is a low-cost, reusable adsorbent well suited to stripping cationic dyes from wastewater.

How to cite this article
Mohammed Najem W. Synthesis and Structural Characterization of a Zeolite-Incorporated Carboxymethyl Cellulose Hydrogel for Safranin O Adsorption: Equilibrium, Kinetics, Thermodynamics and Reusability. J Nanostruct, 2026; 16(4):4890-4900.
DOI: 10.22052/JNS.2026.04.035

INTRODUCTION

Pollution of water by synthetic dyes is still a serious problem for industrialized and developing countries alike. Every year the textile, leather, paper, and food-processing sectors release large quantities of coloured effluent into rivers and lakes, and the resulting harm runs from eutrophication to outright aquatic toxicity [1,2]. An example of such a dye is Safranin O (Saf; $C_{20}H_{19}ClN_4$; λ_{max} = 520 nm), a cationic phenazine dye used for biological staining, textile finishing and as a redox indicator. The aromatic framework that renders it chemically stable and light-fast, also explains its recalcitrance to biodegradation, its toxicity to aquatic life and to humans in whom it has been associated with mutagenic, carcinogenic

* *Corresponding Author Email: walaa.m.najem@jmu.edu.iq*

and DNA-damaging effects [3,4]. The phenazine skeleton of Saf belongs to the wider family of nitrogen-containing heterocycles, a class of compounds that is extensively synthesised and screened for biological activity, in line with the toxicological concerns noted above [5,6]. There are several ways proposed for the removal of dyes from water including advanced oxidation, membrane filtration, electrochemical treatment and biological process [7,8]. Each of them has its advantages, but adsorption is still of interest due of its simplicity, low cost of installation and wide application to pollutants [9]. Among these adsorbents, carbons obtained from natural, low-cost precursors, including activated and nano-structured forms, have been widely reviewed as effective materials for water treatment [10]. Much of the recent work has focused on adsorbents derived from renewable biodegradable polymers, particularly hydrogels, because their three-dimensional crosslinked networks swell in water and offer functional groups (hydroxyl, carboxyl, amide) which bind cationic species [11,12].

Carboxymethyl cellulose (CMC) is a water-soluble derivative of cellulose, which is biocompatible, low cost and has a high density of carboxylate groups, making it an ideal backbone for hydrogels [13]. CMC is grafted with vinyl monomers such as acrylic acid (AAc) and hydroxyethyl acrylamide (HEAM) via free-radical polymerisation to create additional ionisable sites and make the gel mechanically stronger [14]. In contrast, the purely organic hydrogels usually have a small surface area and moderate temperature stability only. The addition of an inorganic filler, in particular zeolite (a microporous aluminosilicate, which is an ion exchanger and has a high specific surface area) can overcome these drawbacks, leading to an organic-inorganic nanocomposite with improved adsorption properties than the separate components [15,16].

Publications on hydrogel adsorbents are growing rapidly, but there are comparatively few publications on a ternary system of CMC, two-monomer graft (AAc + HEAM) and natural zeolite for safranin O. Published work has focused on methylene blue and crystal violet, thus Saf has been less studied, regardless of the fact that its rigid structure and nitrogen-rich framework may react differently on a mixed-functional surface [17,18]. Another disadvantage is that many articles give isotherm and kinetic data, but do not carry out a proper nano-characterization or any test of regeneration, so it is difficult to determine how practical the material actually is. With that in mind, the aims of this study were to (i) prepare the (CMC-AAC-co-HEAM)-g-zeolite composite hydrogel by free-radical graft polymerization; (ii) characterize it in detail by FTIR, XRD, FESEM, TEM, BET, TGA, and zeta potential; (iii) measure its batch adsorption of Saf while varying contact time, pH, temperature, adsorbent dose, and ionic strength; (iv) fit the equilibrium, kinetic, and thermodynamic data to suitable models; and (v) check how well it holds up over repeated use.

MATERIALS AND METHODS

Chemicals and reagents

Sodium carboxymethyl cellulose (CMC, M. wt ≈ 250,000, DS ≈ 0.7), hydroxyethyl acrylamide (HEAM, 99.0%), acrylic acid (AAc, 99.0%), and safranin O (Saf, $C_{20}H_{19}ClN_4$, M. wt = 350.85 g mol^{-1}, purity > 95%) were all supplied by Himedia (India). N, N′-Methylenebisacrylamide (MBA, 99.0%) and potassium persulfate (KPS, 99.5%) came from CDH (India). The natural zeolite was of the clinoptilolite type and obtained from a commercial supplier. Hydrochloric acid (37%), sodium hydroxide, NaCl, KCl, and $CaCl_2$ were all analytical grade, and every solution was made up in deionized water.

Preparation of the hydrogel composite

The composite was made in a single pot by free-radical graft polymerization. In a representative run, 1.0 g of CMC powder was dissolved in 50 mL of deionized water and stirred magnetically (120 rpm) at 50 °C for 30 min in a 250 mL three-neck round-bottom flask equipped with a reflux condenser, a thermometer, and a nitrogen inlet. After complete dissolution, 4 mL of HEAM was added and agitated until homogenous, then 4 mL of AAc was added dropwise at 25 °C. The crosslinker MBA (0.01 g in 2 mL water) was added slowly with stirring over 5 min and then the initiator KPS (0.01 g in 2 mL water) was added to initiate the production of radicals. 0.01 g of zeolite (dispersed in water (10 mL) by sonication for 10 min) was added dropwise. The mixture was then heated up to 70 °C in a water-bath, kept at this temperature for 3 h under nitrogen. The gel obtained was washed multiple times with deionised water to remove unreacted monomer, dried at 60 °C for 48 h then crushed and sieved. As a control, a plain hydrogel was made in the same way but without zeolite.

Characterization techniques

The FTIR spectra were acquired on KBr pellets in the range 400-4000 cm^{-1} using a Shimadzu 8400S. X-ray diffraction patterns (XRD, Shimadzu XRD-6000, Cu-Kα, λ = 1.5406 Å) were measured in the range of 2θ = 8-80°. The morphology was studied by using TESCAN MIRA3 field emission scanning electron microscope (FESEM) and LEO 912AB transmission electron microscope (TEM). The specific surface area and BJH pore-size distribution were measured by using nitrogen adsorption-desorption isotherms obtained on a Quantachrome NOVA 2200e. Thermal stability was checked by TGA (Perkin Elmer TGA4000) under N_2 at a heating rate of 10 °C min^{-1} from room temperature up to 983 °C. Zeta potentials were evaluated in the pH range of 2-12 using a Malvern Zetasizer Nano ZS (Malvern Panalytical Ltd., Malvern, UK. Saf concentrations were quantified by UV-Vis absorption with a Shimadzu UV-1800 spectrophotometer at λ_{max} = 520 nm.

Batch adsorption experiments

All adsorption experiments were conducted in batch mode. A fixed concentration of Saf solution was prepared in a glass vial containing a weighed amount of composite (often 0.02 g) and shaken at 120 rpm. After the contact period, the suspension was centrifuged (6000 rpm, 10 min) and the absorbance of the supernatant was measured at 520 nm. The adsorption capacity (q_e, mg/g) and the removal efficiency (%R) were then calculated from the conventional expressions:

$$q_e = (C_o - C_e) * V / m \quad (1)$$

$$\%R = [(C_o - C_e)/ C_o] * 100 \quad (2)$$

where C_o and C_e are the initial and equilibrium dye concentrations (mg/ L), V is the volume of solution (L), and m is the mass of adsorbent (g).

Contact time was studied from 0 to 120 min (C_o = 300 mg L^{-1}, pH 7, 25 °C), while the adsorbent dose was changed from 0.01 to 0.09 g. The pH was set anywhere between 2 and 11 with 0.1 M HCl or NaOH. For the isotherms, the temperature was varied over 5-35 °C using initial concentrations of 200-500 mg L^{-1}. To probe ionic strength, NaCl, KCl, and $CaCl_2$ were each used at 0.01-0.20 mol L^{-1}. Reusability was checked over four successive adsorption-desorption cycles with 0.1 M HCl as the eluent.

Isotherm and kinetic modeling

The equilibrium data were treated with the Langmuir, Freundlich, and Temkin isotherm models, and the kinetic data with the pseudo-first-order (PFO) and pseudo-second-order (PSO)

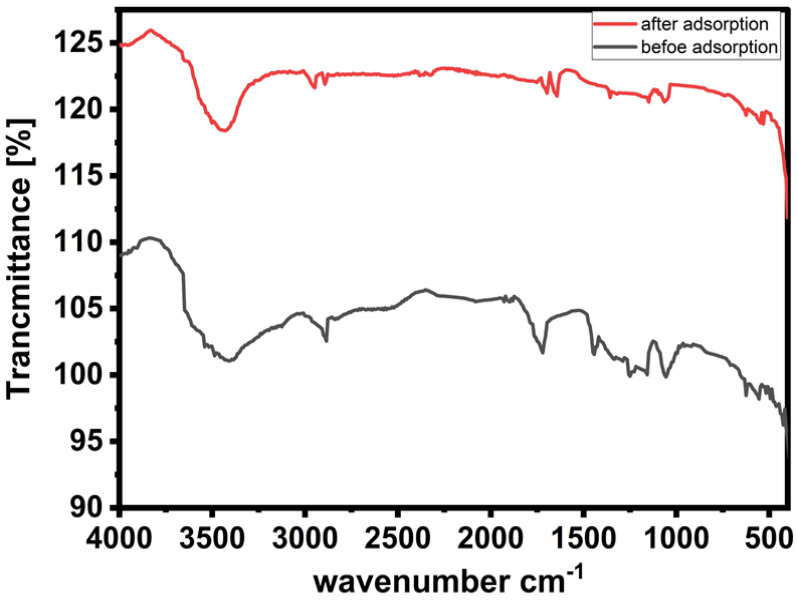

Fig. 1. FTIR spectra of the (CMC-AAC-co-HEAM)-g-zeolite composite before and after safranin O adsorption.

models. Thermodynamic quantities (ΔG, ΔH, ΔS) were obtained from the van't Hoff equation by plotting ln X_m against 1/T [19,20].

RESULTS AND DISCUSSION

Structural and morphological characterization

The FTIR spectra of the composite before and after Saf uptake are shown in Fig. 1. In the pristine material a broad band sat at 3409 cm^{-1}, which we assign to overlapping O-H stretching of CMC and HEAM together with N-H vibrations from MBA and HEAM [21]. The clear absorption at 1720 cm^{-1} belongs to the carbonyl stretch of the ester, amide, and carboxyl groups brought in by the grafted monomers, and the band at 2885 cm^{-1} to aliphatic C-H_2 stretching; the features at 1249 and 1157 cm^{-1} correspond to C-N and C-O stretches, respectively. The bands at 1064 and 555 cm^{-1} are the ones that confirm zeolite has been built into the network, arising from asymmetric Si-O-Si stretching and Al-O-Si bending [22]. That no vinyl C=C peak appears near 1600 cm^{-1} tells us the monomer double bonds were fully consumed during polymerization. Adsorption of Saf brought a few changes worth noting: the broad O-H/N-H band moved to 3448 cm^{-1} and lost intensity, which is consistent with hydrogen bonding between the composite's functional groups and the amino groups of the dye. The aromatic C=C vibrations of the bound Saf resulted in the appearance of a new band at 1627 cm−1, and the carbonyl peak shifted from 1720 to 1689 cm−1, suggesting the direct involvement of the carboxylate groups in the binding of the dye [23].

The XRD trace of plain hydrogel displayed a broad diffuse hump at 2θ = 21.4° which is typical of amorphous crosslinked polymer (Fig. 2). The halo still presented in the composite with weak peaks at 2θ = 9.85°, 22.1° and 29.2° which are in agreement with the crystalline clinoptilolite phase [24]. These zeolite reflections were substantially weaker than those of pure zeolite, suggesting that the zeolite is dispersed as a distinct phase throughout the amorphous gel rather than as discrete clumps. In fact, it is beneficial to keep the amorphous nature for adsorption, since a disordered, open network allows dye molecules to seep in more easily.

Before adsorption, the FESEM images (Fig. 3a, b) showed a rough, very porous surface dotted with cavities and folds of irregular size. This kind of texture, which the zeolite helps create, opens several routes for the adsorbate to travel and enlarges the area actually available for contact. Once Saf had been taken up (Fig. 3c, d) the

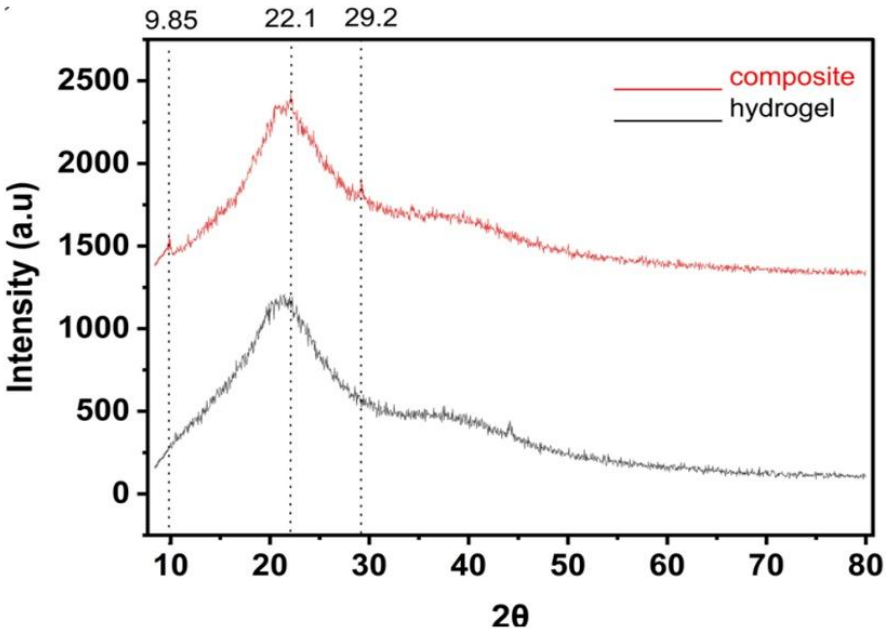

Fig. 2. XRD patterns of the (CMC-AAC-co-HEAM) hydrogel and its zeolite composite, showing the amorphous polymer halo together with the clinoptilolite reflections at 2θ = 9.85°, 22.1°, and 29.2° in the composite

surface looked distinctly smoother and the pores were harder to make out, in line with pores being filled and the surface being covered by dye [25]. The TEM images (Fig. 3e, f) showed zeolite nanoparticles scattered through the polymer, clustered here and there, which confirms they are genuinely embedded. It is likely the combination of the zeolite's microporous framework with the hydrogel's larger channels that gives the composite its good adsorption behaviour.

Surface area, pore structure, and surface charge

The nitrogen adsorption-desorption isotherms were Type IV with H3 hysteresis, which marks both the hydrogel and its composite as mesoporous [26]. Adding zeolite raised the BET surface area from 8.243 $m^2 g^{-1}$ for the plain hydrogel to 9.801 $m^2 g^{-1}$ for the composite, and the total pore volume from 0.00567 to 0.00675 $cm^3 g^{-1}$ (Fig. 4a and Table 1). These numbers are small next to those of activated carbons, but they reflect only the polymer matrix; in hydrogels it is really the density of functional groups, not the surface area on its own, that governs how much dye is taken up [27]. BJH analysis put the mean pore diameter near 2.75 nm, within the mesopore range (2-50 nm by the IUPAC scheme), wide enough for the fairly bulky Saf molecule (MW = 350.85 g mol^{-1}) to move into the interior of the gel.

The point of zero net charge (pH_{zpc}) of the composite was found to be 3.8. Above this pH the surface grows steadily more negative as the carboxyl and hydroxyl groups ionize, which pulls the cationic Saf toward it. Below 3.8 the groups are protonated and the surface carries a net positive charge that pushes the cationic dye away, and this fits the low uptake seen under strongly acidic conditions (Fig. 4b). The zeta potential results thus back up the pH-dependent adsorption behaviour described in Section 3.4 [28].

Gel content and swelling behavior

The gel fraction worked out at 99.95% for the plain hydrogel and 99.93% for the composite, which means monomer conversion was almost total and the network tightly crosslinked. Values this high show that the KPS/MBA pair propagated radicals efficiently and that the small amount of zeolite did nothing to hold back crosslinking [29]. In the swelling tests the composite took up far more water at basic pH than at acidic pH, with a maximum around pH 8. The reason is that above their pKa the carboxyl groups ionize to COO^-; these charged groups repel one another, the network expands, and more water, along with dissolved pollutant, can work its way inside [30].

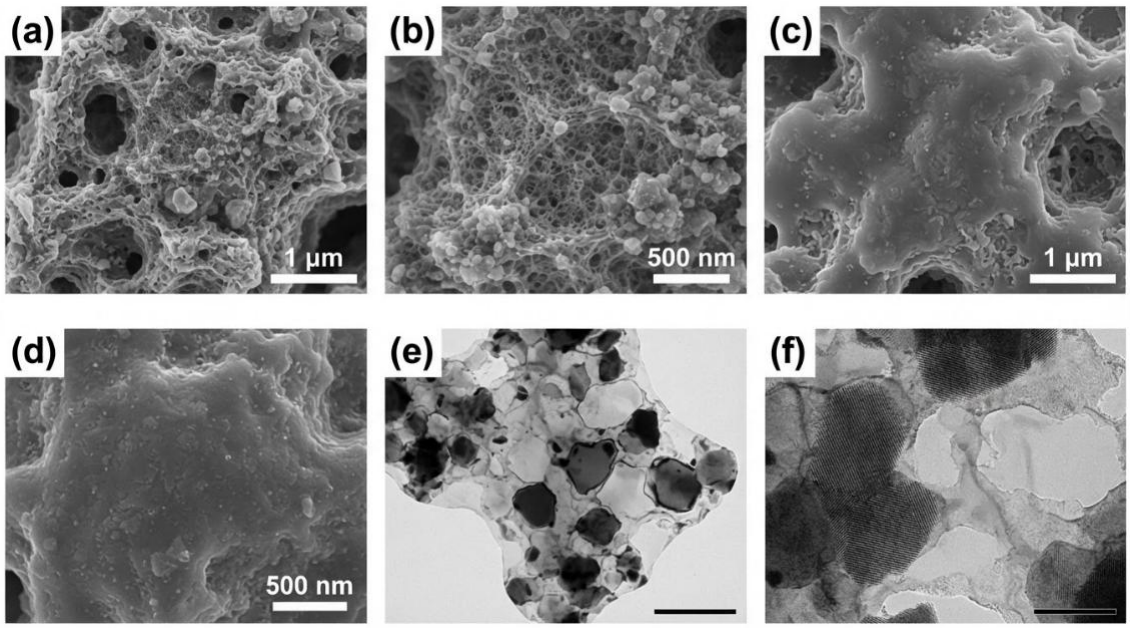

Fig. 3. (a, b) FESEM images of the composite before Saf adsorption at 1 µm and 500 nm; (c, d) after Saf adsorption; (e, f) TEM images of the composite at different magnifications.

Effect of contact time and adsorption kinetics

Fig. 5a follows Saf uptake on the composite over time at 25 °C (C_o = 300 mg L^{-1}, 0.02 g adsorbent, pH 7). The dye was taken up quickly in the first 20 min, more slowly between 20 and 45 min, and had essentially levelled off by about 60 min, so 60 min was adopted as the equilibrium time. There are numerous empty sites early on and a big concentration gradient, which explains the quick start; when those sites fill and diffusion inside the particles becomes limiting, the rate falls off [31].

The kinetic data were fitted to the PFO and PSO models to determine the rate controlling process. This is clearly presented in Fig. 6 and Table 2. The PSO model was fitted almost perfectly (R 2 = 1.000) and its calculated equilibrium capacity ($q_{e,calc}$ = 149.254 mg/g) was close to the measured value. The PFO fit was bad (R^2 = 0.891) and substantially overestimated q_e. A PSO fit of this grade indicates the prevalence of chemisorption type interactions, mainly electrostatic attraction and hydrogen bonding between the anionic groups of the composite and the cationic dye [32]. The initial rate h was 312.5 mg g^{-1} min^{-1} suggesting easy affinity of Saf to the surface.

Effect of pH

Solution pH has a strong effect on how much cationic dye is adsorbed, because it changes both the charge on the adsorbent and the form the dye takes in solution. Fig. 5b shows Saf uptake climbing steadily as the pH went from 2 to 9 and then dropping back a little past that. At low pH the carboxyl and hydroxyl groups are protonated, the surface carries a positive charge, and the cationic Saf is repelled. Once the pH climbs above the pH_{zpc} (3.8), stepwise deprotonation leaves the surface negatively charged and it now attracts the dye, which accounts for the rising curve [33]. The little dip above pH 9 might be because the dye's own amino groups are losing protons, reducing the coulombic attraction, or it might just be the torrent

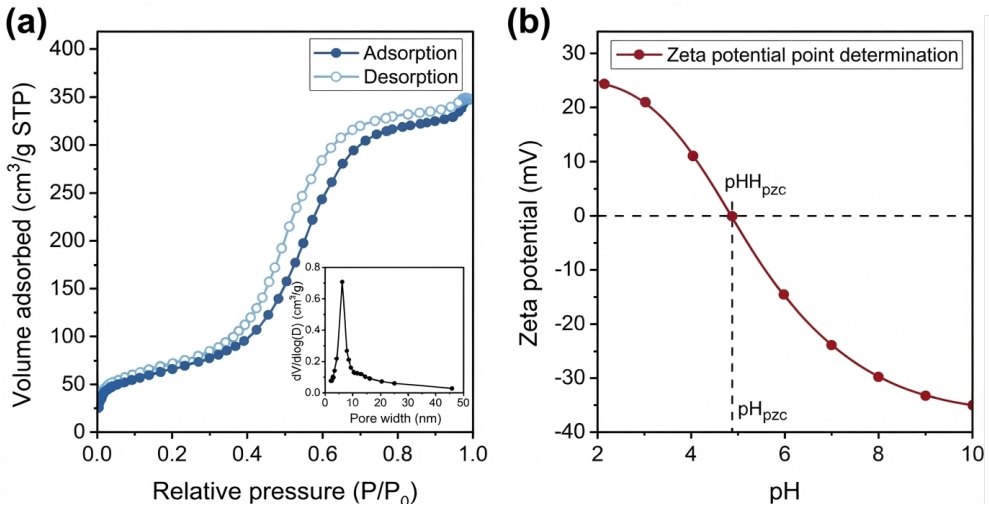

Fig. 4. (a) N_2 adsorption-desorption isotherms (BET) and BJH pore-size distribution (inset) for the composite; (b) Zeta potential versus p

Table 1. Textural properties of the hydrogel and its zeolite composite from BET/BJH analysis.

Property	Hydrogel	Composite
BET surface area (m^2/g)	8.243	9.801
Pore volume (cm^3/g)	0.00567	0.00675
Mean pore diameter (nm)	≈2.75	≈2.75
Isotherm type	IV (H3)	IV (H3)

of OH^- ions contending for the surface. Based on that, pH 9 was selected as best, while the rest of the trials done at pH 7 to be close to near neutral circumstances of real water.

Adsorption isotherms

The equilibrium values at 25 °C were fitted to the Langmuir, Freundlich and Temkin equations for starting Saf concentrations in the range of 200-500 mg/L. The linearised fits are compared in Fig. 7 and the parameters are listed in Table 3. Freundlich provided the best correlation followed by Temkin and Langmuir with R^2 = 0.9869, 0.9648 and 0.9374 respectively. The best fitting to Freundlich model indicates a heterogeneous surface where the sites are not all energetically equivalent and the covering occurs in more than one layer, which is in agreement with the mixed organic-inorganic nature of the composite [34]. Adsorption was favourable with an intensity parameter n = 2.206 (> 1) and the capacity factor K_F = 99.51 mg/g (mg/L) (1/n) showed a high affinity. The Langmuir fit, although weaker, still produced a maximum monolayer capacity of q_m = 271.19 mg g^{-1}, a convenient number to compare with other adsorbents (Table 3). The Temkin constant B = 66.45 J mol^{-1} is related to the heat of adsorption and, given the context of the thermodynamic data (Section 3.7), is compatible with adsorption that is physical but with an electrostatic component [35,36].

Temperature effect and thermodynamic evaluation

The adsorption was conducted at four different temperatures (5, 15, 25, 35 °C) and different beginning concentrations (200-500 mg/L). The capacity slowly decreased with the increase in temperature (Fig. 8a). The maximum absorption

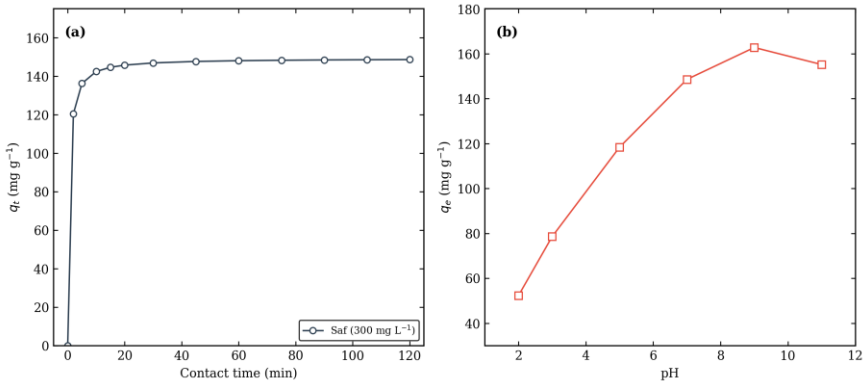

Fig. 5. (a) Effect of contact time on safranin O adsorption (C_o = 300 mg L^{-1}, 0.02 g, pH 7, 25 °C); (b) Effect of solution pH on q_e (C_o = 300 mg L^{-1}, 60 min, 25 °C).

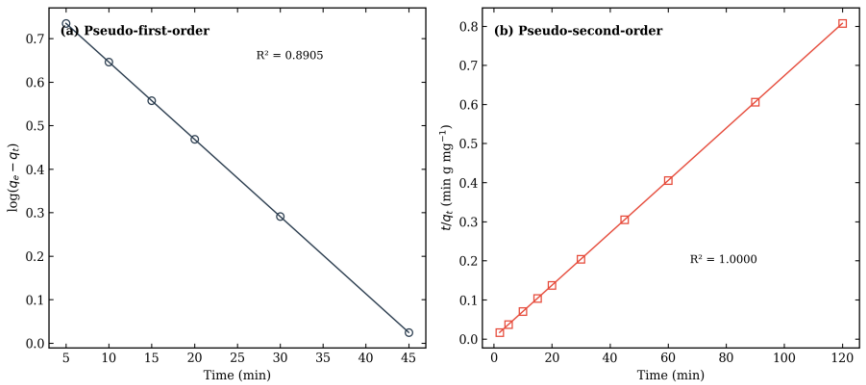

Fig. 6. Linearized kinetic plots for Saf adsorption: (a) pseudo-first-order; (b) pseudo-second-order.

was decreased from 248.8 mg/g at 5 °C to 235.9 mg/g at 35 °C. Such an inverse dependence is common for an exothermic process, in which the added heat energy disrupts the weak physical connections between the dye and the surface, and by increasing solubility of dye, shifts equilibrium back toward solution [37].

The thermodynamic parameters were obtained from the Van't Hoff plot of ln X_m vs. 1/T (Fig. 8b) and are presented in Table 4. The exothermic nature is quantified by the negative enthalpy (ΔH = −58.76 kJ/mol) and the negative ΔG for the temperatures tested, confirms the spontaneity of the activity. The negative entropy shift (ΔS = −165.1 J/ K.mol) indicates that the solid-liquid interface becomes more ordered after the Saf binding, as expected for the formation of an ordered dye-surface complex. Note that the value of ΔH is greater than the 40 kJ/mol figure commonly used to distinguish between physisorption and chemisorption, so the binding is unlikely to be purely van der Waals but a mixture of electrostatic attraction, hydrogen bonding and possibly π-π stacking between the aromatic rings of Saf and the polymer backbone [38,39]. This mixed mechanism interpretation is consistent with the FTIR alterations seen upon

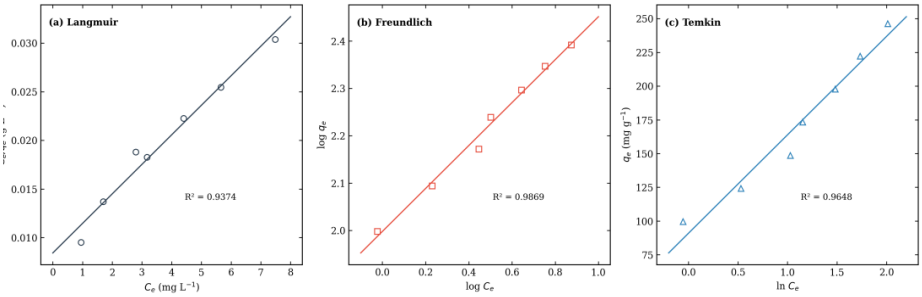

Fig. 7. Linearized isotherms for Saf on the composite at 25 °C: (a) Langmuir; (b) Freundlich; (c) Temkin.

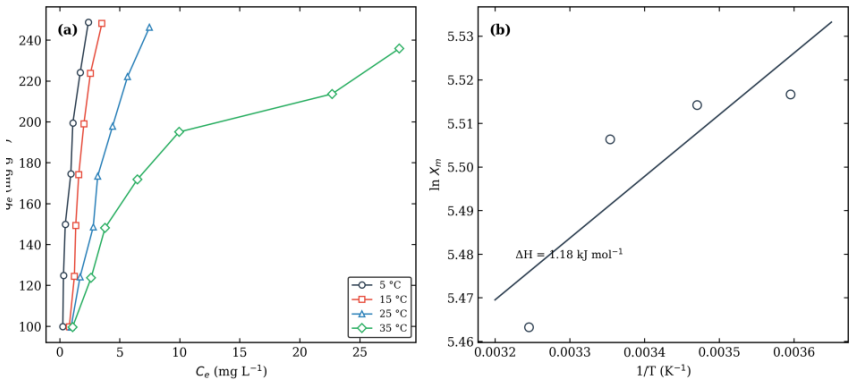

Fig. 8. (a) Effect of temperature on Saf isotherms (pH 7, 0.02 g, 60 min); (b) Van't Hoff plot (ln X_m vs. 1/T).

Table 2. Kinetic parameters for safranin O adsorption on the composite (C_o = 300 mg L^{-1}, 25 °C).

Model	Parameter	Value	R^2
PFO	q_e (mg/g)	6.664	0.891
PSO	q_e (mg/g)	149.254	1.000
PSO	k_2 (g/mg·min)	0.01403	—
PSO	h (mg/g·min)	312.5	

adsorption and the PSO kinetics.

Ionic strength effect and reusability

The competing cations were evaluated by adding 0.01-0.20 mol/L of NaCl, KCl or $CaCl_2$ (Fig. 9a). In all cases salt decreased capacity, $CaCl_2$ being the most damaging followed by NaCl and then KCl. The divalent Ca^{2+} ion has a greater contribution to the ionic strength per mole than the monovalent one and a better competition for the negatively charged sites, pushing Saf off the surface. This sensitivity of the primary adsorption mechanism to ionic strength is itself a proof of the electrostatic nature of the process [40].

The material was well regenerated in four adsorption-desorption cycles with 0.1 M HCl, and the removal efficiency was only reduced slightly from 99.1% in the first cycle to 87.4% in the fourth cycle (Fig. 9b). That modest reduction is due to loss of a portion of the accessible sites, and slight

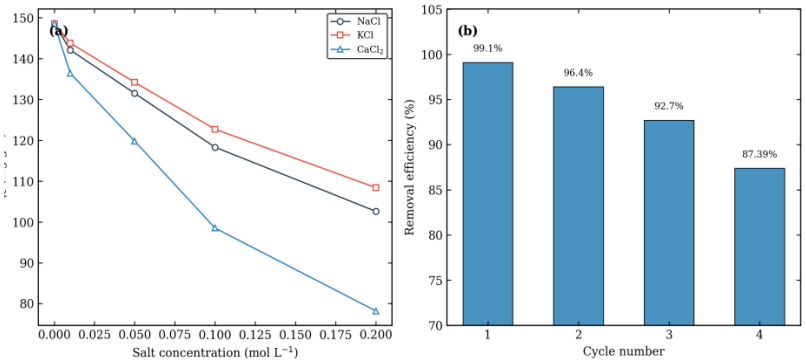

Fig. 9. (a) Effect of ionic strength on Saf adsorption (NaCl, KCl, $CaCl_2$; C_o = 300 mg L^{-1}, 25 °C); (b) Removal efficiency over four adsorption-desorption cycles with 0.1 M HCl.

Table 3. Isotherm parameters for safranin O adsorption on the composite at 25 °C.

Model	Parameter	Value	R^2
Langmuir	q_m (mg/g)	271.19	0.9374
	K_L (L/mg)	0.5114	—
Freundlich	K_F	99.514	0.9869
	N	2.206	—
Temkin	B (J/mol)	66.449	0.9648
	K_T (L/g)	3.929	—

Table 4. Thermodynamic parameters for safranin O adsorption on the composite.

Parameter	Value	Unit	Interpretation
ΔH	−58.76	kJ/mol	Exothermic
ΔS	−165.1	J/K·mol	Ordered binding
ΔG (25 °C)	−10.37	kJ/mol	Spontaneous

Table 5. Comparison of Saf adsorption capacities of various adsorbents.

Adsorbent	q_m (mg/g)	Ref.
(CMC-AAC-co-HEAM)-g-zeolite	271.19	This work
Alginate/polypyrrole composite	175.44	[39]
Pectin-g-pAA/clay nanocomposite	210.30	[40]
Gellan gum/itaconic acid hydrogel	198.50	[41]
CMC-g-pAA/bentonite	243.90	[42]

structural relaxation in the gel, but the remainder is still high enough for genuine column or batch application. HCl worked better than NaOH or ethanol, most likely because in acid the COO^- and NH groups pick up protons, the electrostatic hold on the cationic dye weakens, and the dye comes off more easily [41].

Comparison with other adsorbents

Table 5 sets the capacity of the present composite against a selection of adsorbents from the recent literature. Its q_m of 271.19 mg g^{-1} holds up against, and in a few cases beats, figures reported for carbon-based, clay-based, and other polymeric adsorbents, which speaks to the value of pairing a swellable hydrogel with the ion-exchange capacity of zeolite [42-45].

CONCLUSION

A zeolite-grafted biopolymer composite, (CMC-AAC-co-HEAM)-g-zeolite, was prepared by free-radical graft polymerization and characterized in some detail for its nano-scale structure and surface chemistry. It removed safranin O from water effectively, reaching a Langmuir maximum capacity of 271.19 mg g^{-1} and coming to equilibrium inside 60 min. The uptake followed pseudo-second-order kinetics and the Freundlich isotherm, which places the rate-limiting step at surface interactions on an energetically uneven surface. The thermodynamics were exothermic and spontaneous, driven by electrostatic attraction, hydrogen bonding, and probably some π-π interaction between the aromatic part of the dye and the polymer backbone. Dilute HCl regenerated the material easily, and about 87% of the original removal efficiency survived four cycles. On the whole, then, this zeolite-enhanced hydrogel is a cheap, reusable, and effective adsorbent for pulling cationic dyes out of contaminated water. Sensible next steps would be to test it in a fixed-bed column, to look at competition when several pollutants are present, and to weigh up scale-up under genuine wastewater conditions.

CONFLICT OF INTEREST

The authors declare that there is no conflict of interests regarding the publication of this manuscript.

REFERENCES

1. Mushtaq B. Industrial Growth and Ecological Degradation in Asia: Evidence from a Multidimensional Pollution Index. Global Business Review. 2026.
2. Khan S, Ajmal S, Hussain T, Rahman MU. Clay-based materials for enhanced water treatment: adsorption mechanisms, challenges, and future directions. Journal of Umm Al-Qura University for Applied Sciences. 2023;11(2):219-234.
3. Agbasi JC, Chukwu CN, Nweke ND, Uwajingba HC, Khan MYA, Egbueri JC. Water pollution indexing and health risk assessment due to PTE ingestion and dermal absorption for nine human populations in Southeast Nigeria. Groundwater for Sustainable Development. 2023;21:100921.
4. Al-Musawi TJ, Mengelizadeh N, Kassim WMS, Sillanpää M, Siddiqui SH, Shahbaksh S, et al. Sonophotocatalytic degradation and operational parameters optimization of diazinon using magnetic cobalt–graphene nanocomposite as a catalyst. Journal of Water Process Engineering. 2022;46:102548.
5. Al-Suraify SMT, Hussien LB. RETRACTED ARTICLE: Synthesis and characterization of new compounds derived from 1H-indol-5-ylamine. Applied Nanoscience. 2022;13(3):2083-2092.
6. Shaimaa hatem A. Synthesis, diagnosis and biological activity study of some heterocyclic compounds derived from 2-aminobenzothiazole. Tikrit Journal of Pure Science. 2018;23(4):32-38.
7. Chen X, Boo C, Yip NY. Transport and structural properties of osmotic membranes in high-salinity desalination using cascading osmotically mediated reverse osmosis. Desalination. 2020;479:114335.
8. Wolkersdorfer C. Valanko et al.: About Water Treatment (Book Review). Mine Water Environ. 2021;40(3):803-804.
9. Heybet EN, Ugraskan V, Isik B, Yazici O. Adsorption of methylene blue dye on sodium alginate/polypyrrole nanotube composites. Int J Biol Macromol. 2021;193:88-99.
10. Ali AA, Tawalbeh M, Al-Othman A. Water Treatment Applications of Green Polymers. Comprehensive Green Materials: Elsevier; 2025. p. 453-469.
11. Sharma G, Kumar A, Chauhan C, Okram A, Sharma S, Pathania D, et al. Pectin-c rosslinked -guar gum/SPION nanocomposite hydrogel for adsorption of m-cresol and o-chlorophenol. Sustainable Chemistry and Pharmacy. 2017;6:96-106.
12. Abbasi A, Ahmad I, Ikram S. Exploration of Adsorption Efficiency Mechanism and Swelling Behavior of Novel Green Itaconic Acid Modified Gellan Gum Hydrogel Nanocomposite for the Removal of Noxious Dyes. Journal of Polymers and the Environment. 2023;32(4):1684-1705.
13. Rahman MM, Ihara H, Takafuji M. Nanomaterial Hybridized Hydrogels as a Potential Adsorbent for Toxic Remediation of Substances from Wastewater. Recent Trends in Wastewater Treatment: Springer International Publishing; 2022. p. 365-393.
14. El-Hag Ali A. Removal of heavy metals from model wastewater by using carboxymehyl cellulose/2-acrylamido-2-methyl propane sulfonic acid hydrogels. J Appl Polym Sci. 2011;123(2):763-769.
15. Ren H, Gao Z, Wu D, Jiang J, Sun Y, Luo C. Efficient Pb(II) removal using sodium alginate–carboxymethyl cellulose gel beads: Preparation, characterization, and adsorption mechanism. Carbohydr Polym. 2016;137:402-409.
16. Ankrah AF, Tokay B, Snape CE. Heavy Metal Removal from Aqueous Solutions Using Fly-Ash Derived Zeolite

NaP1. International Journal of Environmental Research. 2022;16(2).
17. Gómez F, Galil B. Comments on the "Mediterranean alien harmful algal blooms" by Marampouti et al. Environ. Sci. Pollut. Res. 2021. Environmental Science and Pollution Research. 2021;28(41):58810-58811.
18. Hosseinzadeh H, Bahador N. Novel CdS quantum dots templated hydrogel nanocomposites: Synthesis, characterization, swelling and dye adsorption properties. J Mol Liq. 2017;240:630-641.
19. Lima EC, Hosseini-Bandegharaei A, Moreno-Piraján JC, Anastopoulos I. A critical review of the estimation of the thermodynamic parameters on adsorption equilibria. Wrong use of equilibrium constant in the Van't Hoof equation for calculation of thermodynamic parameters of adsorption. J Mol Liq. 2019;273:425-434.
20. Tran HN, You S-J, Chao H-P. Thermodynamic parameters of cadmium adsorption onto orange peel calculated from various methods: A comparison study. Journal of Environmental Chemical Engineering. 2016;4(3):2671-2682.
21. CO2Activated Adsorption: A New Approach to Dye Removal by Chitosan Hydrogel. American Chemical Society (ACS). http://dx.doi.org/10.1021/acsomega.8b01825.s001
22. Characterization II. Molecular Sieves: Springer Berlin Heidelberg; 2007. http://dx.doi.org/10.1007/b58179
23. Al-Hazmi GAA, El-Bindary MA, El-Desouky MG, El-Bindary AA. Efficient adsorptive removal of industrial dye from aqueous solution by synthesized zeolitic imidazolate framework-8 loaded date seed activated carbon and statistical physics modeling. Desalination and Water Treatment. 2022;258:85-103.
24. Treacy MMJ, Higgins JB. RUB-24. Collection of Simulated XRD Powder Patterns for Zeolites: Elsevier; 2007. p. 366-367.
25. Ehsani P, Farahpour MR, Mohammadi M, Mahmazi S, Jafarirad S. Green fabrication of ZnO/magnetite-based nanocomposite - using Salvia officinalis extract with antibacterial properties enhanced infected full-thickness wound. Colloids Surf Physicochem Eng Aspects. 2021;628:127362.
26. Thommes M, Kaneko K, Neimark AV, Olivier JP, Rodriguez-Reinoso F, Rouquerol J, et al. Physisorption of gases, with special reference to the evaluation of surface area and pore size distribution (IUPAC Technical Report). Pure and Applied Chemistry. 2015;87(9-10):1051-1069.
27. Ali I, Asim M, Khan TA. Low cost adsorbents for the removal of organic pollutants from wastewater. J Environ Manage. 2012;113:170-183.
28. Slokar YM, Majcen Le Marechal A. Methods of decoloration of textile wastewaters. Dyes and Pigments. 1998;37(4):335-356.
29. Bordoloi N, Dutta N, Thakur S, Dutta P. Cellulose-based hydrogels in food industry. Cellulose-Based Hydrogels: Elsevier; 2025. p. 413-437.
30. Druel L, Budtova T. Aerogel-like (low density and high surface area) cellulose monoliths and beads obtained without supercritical- or freeze-drying. Cellulose. 2023;30(13):8339-8353.
31. Ho YS, McKay G. A Comparison of Chemisorption Kinetic Models Applied to Pollutant Removal on Various Sorbents. Process Saf Environ Prot. 1998;76(4):332-340.
32. Simonin J-P. On the comparison of pseudo-first order and pseudo-second order rate laws in the modeling of adsorption kinetics. Chem Eng J. 2016;300:254-263.
33. Chandane V, Singh VK. Adsorption of safranin dye from aqueous solutions using a low-cost agro-waste material soybean hull. Desalination and Water Treatment. 2016;57(9):4122-4134.
34. Foo KY, Hameed BH. Insights into the modeling of adsorption isotherm systems. Chem Eng J. 2010;156(1):2-10.
35. Sasa Y, Uda M, Toyoshima I. The Crystallite Size of A-Iron in the Presence of K_2O in the Doubly Promoted Ammonia Synthesis Iron Catalysts. Chem Lett. 1982;11(12):2011-2014.
36. Al-Ghouti MA, Da'ana DA. Guidelines for the use and interpretation of adsorption isotherm models: A review. J Hazard Mater. 2020;393:122383.
37. Al-Harby NF, Albahly EF, Mohamed NA. Kinetics, Isotherm and Thermodynamic Studies for Efficient Adsorption of Congo Red Dye from Aqueous Solution onto Novel Cyanoguanidine-Modified Chitosan Adsorbent. Polymers. 2021;13(24):4446.
38. Guo X, Wang J. Comparison of linearization methods for modeling the Langmuir adsorption isotherm. J Mol Liq. 2019;296:111850.
39. Wang S, Peng Y. Natural zeolites as effective adsorbents in water and wastewater treatment. Chem Eng J. 2010;156(1):11-24.
40. Figure 3: Effect of ionic strength on adsorption of Tl by rutile nano-TiO_2. PeerJ. http://dx.doi.org/10.7717/peerj.6820/fig-3
41. Cao D, Xu X, Jiang S. Corrigendum to "Ultrasound-electrochemistry enhanced flotation and desulphurization for fine coal" [Sep. Purif. Technol. 258 (2021) 117968]. Sep Purif Technol. 2021;278:119585.
42. Al-Shemy MT, Al-Sayed A, Dacrory S. Fabrication of sodium alginate/graphene oxide/nanocrystalline cellulose scaffold for methylene blue adsorption: Kinetics and thermodynamics study. Sep Purif Technol. 2022;290:120825.
43. Sharma G, Kumar A, Sharma S, Al-Muhtaseb AaH, Naushad M, Ghfar AA, et al. Fabrication and characterization of novel Fe0@Guar gum-crosslinked-soya lecithin nanocomposite hydrogel for photocatalytic degradation of methyl violet dye. Sep Purif Technol. 2019;211:895-908.
44. Özkahraman B, Özbaş Z. Removal of Al(III) Ions Using Gellan Gum-Acrylic Acid Double Network Hydrogel. Journal of Polymers and the Environment. 2019;28(2):689-698.
45. Bulut Y, Karaer H. Removal of Methylene Blue from Aqueous Solution by Crosslinked Chitosan-g-Poly(Acrylic Acid)/Bentonite Composite. Chem Eng Commun. 2014;202(12):1635-1644.